Oxic conditions in shallow marine settings during the Permian-Triassic Mass Extinction

Anja B. Frank[1], Elisabeth L. Warncke-Rüting[1], Stephen E. Grasby[2], Evelyn Kustatscher[3], Herwig Prinoth[4], Simon W. Poulton[5], Yijun Xiong[5], Dieter Korn[6], Jana Gliwa[7], William J. Foster[1]

[1] Universität Hamburg, Institut für Geologie; Hamburg, Germany.

[2] Geological Survey of Canada, Natural Resources Canada; Calgary, Alberta, Canada.

[3] Department of Natural History, Collection and Research Centre (SFZ), Tiroler Landesmuseen, Hall in Tirol, Austria

[4] Museum Ladin; St. Martin in Thurn/San Martino in Badia, South Tyrol, Italy

[5] School of Earth and Environment, University of Leeds; Leeds, UK

[6] Museum für Naturkunde Berlin, Leibniz Institute for Evolution and Biodiversity Science; Berlin, Germany

[7] Freie Universität Berlin, Institut für Geologische Wissenschaften; Berlin, Germany

ABSTRACT

The concept that ultra-shallow marine anoxia was a major cause of the Permian-Triassic mass extinction was partly based on sections from the Dolomites (Italy). We test this hypothesis by re-examining the Dolomites record, utilizing an updated redox sensitive trace metal (V, U and

Mo) approach, combined with Fe speciation and Th/U ratios, and paleontological observations. Redox sensitive trace metal and Fe speciation data reveal fluctuating redox conditions prior to the extinction, with periodic enrichments in highly reactive Fe likely reflecting Fe^{2+} mobilization in anoxic ferruginous deeper waters. Oxic conditions are indicated during and after the extinction event, suggesting that local redox conditions did not control biodiversity changes. However, this redox reconstruction contrasts somewhat with traditional interpretation of Th/U ratios, which indicate more persistent shallow water anoxia, likely due to a strong regional influence of the detrital sediment composition. A comparison with other shallow marine successions reveals similar redox trends, suggesting that shallow water anoxia was not global. Instead, redox conditions across the Permian/Triassic boundary were likely variable, rendering it vital to assess the role of anoxia on a site-specific basis to understand its role in the shallow marine Permian-Triassic mass extinction.

INTRODUCTION

The Permian-Triassic mass extinction (PTME) marks the greatest loss of marine life in the Phanerozoic, with > 90% of marine species going extinct (e.g., Erwin, 1993). Drastic environmental changes associated with the emplacement of the Siberian Traps Large Igneous Province have been proposed as the driving mechanisms behind the extinction (e.g., Grasby and Bond, 2023; Svensen et al., 2023). The release of large volumes of greenhouse gases is hypothesized to have led to a rapid rise in sea surface temperatures, ocean acidification, an increased heavy metal supply, and a spread in ocean anoxia (e.g., Dal Corso et al., 2022; Grasby and Bond, 2023). The expansion of oxygen minimum zones, leading to anoxic or euxinic conditions even in shallow basins, was one of the first proposed extinction drivers (Twitchett and Wignall, 1996; Wignall and Twitchett, 1996). Many subsequent studies have presented

supporting evidence for the development of such conditions during the extinction (Algeo et al., 2007; Grice et al., 2005; Hays et al., 2007; Xiang et al., 2020; Zhang et al., 2020), rendering anoxia a frequently cited driver of the marine extinction. However, in some places the event has been suggested to occur under partially or completely oxic conditions (Algeo et al., 2010; Collin et al., 2015; Foster et al., 2024; Gliwa et al., 2020; Knies et al., 2013; Loope et al., 2013; Proemse et al., 2013; Yang et al., 2024), questioning the importance of anoxia as a global extinction driver.

Considering these variable redox interpretations, it is vital to not only constrain changes in local redox conditions, but also to link these changes to biodiversity changes at the same location, to fully understand the potential role of oxygen availability in the extinction. To address this, we examined the Seis section, a shallow marine Permian-Triassic sedimentary section from the Dolomites, Italy. This is a key section that has been used to suggest that shallow marine anoxia was a key driver of the extinction, based on Th/U ratios, the presence of opportunistic taxa (lingulids and *Claraia*), and pyrite morphologies (Wignall and Twitchett, 1996). However, only post-extinction data have been presented for the Seis section, speaking to a delayed recovery processes, while the critical interval proceeding and during the extinction remain unconstrained.

Currently, there is thus limited evidence for anoxia associated with the mass extinction in the Dolomites, and further study of marine redox conditions prior to and during the event is clearly warranted. To address this, we examined the pre-, during- and post-extinction strata of Seis using redox sensitive trace metals (V, U and Mo), alongside Fe speciation and the previously applied Th/U proxy. We then combine these data with lithological and available

paleontological data to test the hypothesis that anoxia was the main driver of the shallow marine extinction in the western Tethys.

STUDY AREA

The studied section is located in the Dolomites, Italy, at 46.53374, 11.56142 (Fig. 1A) and is known as the Siusi, Seis, Seis/Siusi or Seiser Klamm section (hereafter referred to as Seis). Across the Permian/Triassic boundary (PTB), the Dolomites were part of the Adria tectonic block located near the equator in the western Paleotethys. The Late Permian and Early Triassic sedimentary successions of the Dolomites were deposited in a shallow marine basin on the western margin of the Paleotethys as the Bellerophon and Werfen formations (Fig. 1B). The Bellerophon Formation consists of fossiliferous limestones and dolostones, interbedded with siltstones, sandstones and gypsum (Broglio Loriga et al., 1982; Farabegoli et al., 2007). The overlying Werfen Formation is characterized by shallow marine limestones, dolostones, siltstones and sandstones (Broglio Loriga et al., 1982; Farabegoli et al., 2007) and records the PTME and PTB in its lowermost members (Farabegoli et al., 2007; Posenato, 2019).

METHODS

The Seis section was logged using the formation and unit/member definitions of Broglio Loriga et al. (1982) with some amendments (Fig. 2). A total of 38 samples were taken and analyzed for total organic carbon (TOC) as well as major and trace elements at the Geological Survey of Canada, Calgary. We report redox sensitive trace metal (RSTM) concentrations in terms of enrichment factors (EFs), using the revised method of Krewer et al. (2024) to account for dilution of the detrital input by carbonate (termed EF^{*}). Additionally, iron speciation separation was performed at the University of Leeds. The sum of the extracted Fe phases defines a highly reactive Fe pool (Fe_{Hr}), which when normalized to total Fe (Fe_T) allows oxic conditions

($Fe_{Hr}/Fe_T < 0.22$) to be distinguished from anoxic conditions ($Fe_{Hr}/Fe_T > 0.38$), with intermediate ratios considered equivocal (Poulton and Canfield, 2011). For anoxic samples, pyrite Fe (Fe_{Py}) normalized to Fe_{Hr} further allow ferruginous conditions ($Fe_{Py}/Fe_{Hr} < 0.6$) to be distinguished from euxinia ($Fe_{Py}/Fe_{Hr} > 0.8$), with ratios of 0.6-0.8 considered equivocal (Poulton, 2021). The detailed sample preparation, digestion and analytical techniques as well as the complete geochemical data set are given in the supplemental material[1].

RESULTS AND DISCUSSION

Redox evolution across the PTB

The carbonate-carbon isotope ($\delta^{13}C_{carb}$) record of Seis (Siegert et al., 2011) shows that the negative $\delta^{13}C_{carb}$ excursion indicative of the global environmental perturbations in the Late Permian coincided with the PTME (Fig. 3), supporting the importance of environmental change, such as deoxygenation, for the event. Redox sensitive trace metal contents fluctuate, but consistent patterns appear when the data are expressed as enrichment factors (Fig. 3). The EF_V^* values generally fall close to the baseline of 1 throughout the section, but with a peak at ~2.75 m that coincides with peaks in EF_U^* and EF_{Mo}^*, indicating a particularly enhanced interval of anoxia. A slight decrease in EF_V^* values occurs at ~10.7 m, again consistent with the EF_U^* and EF_{Mo}^* data, indicating a pronounced oxic interval and suggesting fluctuations in oxygenation levels through the pre-extinction interval. Indeed, the EF_U^* and EF_{Mo}^* data, which tend to be more sensitive redox proxies relative to V (see Li et al., 2025), suggest that redox conditions were particularly dynamic during this interval, with regular fluctuations between oxic and anoxic conditions (Fig. 3). This is supported by occasional spikes in TOC, as well as the presence of thin, dark, fine-grained layers interbedded with the carbonates (Figs. 2, 3).

Intervals of elevated Fe_{Hr}/Fe_T with low Fe_{Py}/Fe_{Hr} ratios support periodic development of anoxic ferruginous water column conditions in the pre-extinction phase, likely reflecting mobilization of Fe^{2+} in deeper anoxic waters, followed by precipitation of Fe_{Hr} phases under oxic or dysoxic conditions at the chemocline or following upwelling into oxic shallow waters. Samples with very low Fe_T (< 0.5 wt%), which occur coincident with low TOC contents, have also been suggested to represent oxic depositional conditions (Clarkson et al., 2014), thereby supporting fluctuating redox conditions. These dynamics are further supported by EF_{Mn}^* values (Fig. 3), which show pronounced peaks likely reflecting precipitation of water column Mn during intervals of particularly enhanced shallow water oxygenation. We also note that Fe speciation data reported for the GSSP in south China reveal a similar redox pattern, with large gaps in the record and anoxic signatures leading up to the PTME, taken as evidence for fleeting anoxia (Xiang et al., 2020).

During and after the extinction, however, the RSTM EF^* values persistently fall close to 1 (Fig. 3), suggesting prevailing oxic conditions. Initially low Fe_T contents (< 0.5 wt%) support this interpretation, while a subsequent increase in Fe_{Hr}/Fe_T ratios and EF_{Mn}^* values in tandem, suggests precipitation of reduced Fe and Mn under oxic water column conditions, hence indicating upwelling of deeper anoxic waters into persistently oxic shallower waters.

The Th/U values at Seis (Fig. 3) provide conflicting redox results when considered relative to traditional threshold value of 2, with lower values suggesting anoxia, while ratios of > 2 indicate oxia (Wignall and Twitchett, 1996). While the Th/U ratios shows a considerable variability commonly coinciding with the other redox proxies, they are further highly correlated to the detrital tracer Al ($r = 0.71$). The latter suggests that the redox control of the Th/U might be

partially masked by lithological change, emphasizing the advantage of utilizing EF* in sections with variable detrital content.

Some of the intervals interpreted as being deposited under oxic conditions may in fact reflect dysoxic deposition, since when considered in isolation, none of the applied redox proxies can provide a robust distinction between these two redox states. To evaluate this, we consider an EF_{Mo}^{*} versus EF_{U}^{*} cross-plot (Fig. 4; Tribovillard et al., 2012) in relation to redox trajectories observed in modern redox sensitive marine environments (Li et al., 2025). The data do not generally follow the redox trajectory, which marks the trend that modern dysoxic sediments tend to fall on (Li et al., 2025). Instead, the majority of data plot either in the oxic zone or between the particulate shuttle and redox trajectories, with the latter being typical of fully anoxic sediments (Li et al., 2025). Specifically, the Casera Razzo Member and Ostracod Unit samples generally record EF^{*} systematics typical of anoxic conditions, with the exception of some samples indicative of oxic conditions, supporting redox fluctuations between oxic and fully anoxic. The thin Bulla Member, which occurs just prior to the extinction horizon (see Fig. 2) and is represented by only 1 sample, is somewhat anomalous, in that this sample plots close to the redox trajectory, potentially indicating dysoxic conditions (Fig. 4). The overlying Tesero (marking the PTME) and Mazzin members plot in the region typical of modern oxic sediments (Li et al., 2025).

Taken together, our combined evaluation of multiple redox proxies challenges the suggestion of a sharp swing to anoxic conditions at the beginning of the PTME (Wignall and Twitchett, 1996).

Redox and biodiversity changes

The redox conditions at Seis were highly dynamic prior to the PTME, suggesting that the late Permian ecosystem underwent significant oxygen stress. However, conditions appear to have improved across the extinction horizon itself, questioning the role of anoxia as an extinction trigger in very shallow waters. Further insight into the role of anoxia as an ecological stressor may be gained by relating redox changes to the fossil record. While the redox proxy data support reoccurring anoxia during deposition of the Casera Razzo Member (Figs. 3, 4), its diverse fossil assemblage of algae, foraminifera, ostracods, mollusks and trace fossils (Fig. 2, Broglio Loriga et al., 1988; Cirilli et al., 1998; Farabegoli et al., 2007; Mette and Roozbahani, 2012; Prinoth and Posenato, 2023; Twitchett and Wignall, 1996) required an oxygenated environment. Hence, the anoxic episodes were likely too short-lived to cause long-term uninhabitable conditions. Similarly, the presence of ostracods, bivalves, gastropods and relatively large trace fossils in the Ostracod Unit, as well as bioturbated beds and foraminifera in the Bulla Member (Broglio Loriga et al., 1982; Cirilli et al., 1998; Crasquin et al., 2008; Farabegoli et al., 2007; Foster et al., 2017; Groves et al., 2007; Mette and Roozbahani, 2012), suggest that episodic deoxygenation was not widespread enough to severely impact biodiversity. Since the Ostracod Unit and Bulla Member generally record lower RSTM EF^* values compared to the underlying Casera Razzo Member (Fig. 3), redox conditions and overall stability may have improved leading up to the PTME, questioning the role of anoxia as an extinction cause in this setting.

Role of anoxia as driver of shallow marine extinction during the PTME

Many studies on the PTME present environmental changes identified at one location as a potential global extinction mechanism. However, such an approach may fail to capture spatial heterogeneity in extinction drivers between different water depths, ecosystems and regions. Uranium isotope data suggest a global intensification of anoxia concurrent with the PTME

(Zhang et al., 2020), supported by many sections worldwide. However, the local geochemical signatures at Seis are not consistent with a spread of anoxic waters into shallow waters at this location, suggesting the presence of habitable zones in the western Tethys, which agrees well with previous work from Panthalassa (Algeo et al., 2010; Beatty et al., 2008; Proemse et al., 2013). Considering that the majority of marine fossils preserved in the rock record are found in shallow marine settings, our knowledge of the PTME is mainly based on fossil data from such settings. Hence, if anoxia did not impinge on the shallow western Tethys, it was not the cause of the abrupt disappearance of fossils in this region.

While this might rule out anoxia as the main driver of the PTME in the shallow, western Tethys, deoxygenation could still have been an extinction mechanism elsewhere. Redox evaluations for the eastern Tethys yield heterogenous redox interpretations, but generally support the development of at least episodic deoxygenation (Algeo et al., 2007; Xiang et al., 2020; Yang et al., 2024). However, a recent meta-analysis of available geochemical and fossil data for the GSSP in south China has revealed that temperature rise and nutrient stress were the driving factors of the extinction there, while the role of anoxia has been considered ambiguous (Foster et al., 2024). For the Neotethys, multiple studies have found no evidence for the development of anoxic conditions within shallow carbonate platforms (Collin et al., 2015; Gliwa et al., 2020; Loope et al., 2013). Finally, redox interpretations for Panthalassa support the prevalence of oxic conditions as well as the development of anoxia (Algeo et al., 2010; Grice et al., 2005; Hays et al., 2007; Knies et al., 2013; Proemse et al., 2013). Hence, the timing and degree of deoxygenation was geographically variable, emphasizing that anoxia alone may not have been responsible for the widespread extinction of life in shallow marine basins during the PTME.

ACKNOWLEDGMENTS

WJF and ABF were funded by the DFG grant FO1297/1 and DK and JG by the DFG grant KO1829/18-1 and the Research Unit TERSANE (FOR 2332). The complete geochemical data set is available in the supplemental material[1] and under https://zenodo.org/records/13757436

REFERENCES CITED

Algeo, T.J., Ellwood, B., Nguyen, T.K.T., Rowe, H., Maynard, J.B., 2007. The Permian–Triassic boundary at Nhi Tao, Vietnam: Evidence for recurrent influx of sulfidic watermasses to a shallow-marine carbonate platform. Palaeogeography, Palaeoclimatology, Palaeoecology, The Permian-Triassic Boundary Crisis and Early Triassic Biotic Recovery 252, 304–327. https://doi.org/10.1016/j.palaeo.2006.11.055

Algeo, T.J., Hinnov, L., Moser, J., Maynard, J.B., Elswick, E., Kuwahara, K., Sano, H., 2010. Changes in productivity and redox conditions in the Panthalassic Ocean during the latest Permian. Geology 38, 187–190. https://doi.org/10.1130/G30483.1

Beatty, T.W., Zonneveld, J.-P., Henderson, C.M., 2008. Anomalously diverse Early Triassic ichnofossil assemblages in northwest Pangea: A case for a shallow-marine habitable zone. Geology 36, 771–774. https://doi.org/10.1130/G24952A.1

Broglio Loriga, C., Masetti, D., Neri, C., 1982. La Formazione di Werfen (Scitico) delle Dolomiti occidentali: sedimentologia e biostratigrafia. Associato all'Unione stampa periodica italiana, Milano, Italie.

Broglio Loriga, C., Neri, C., Pasini, M., Posenato, R., 1988. Marine fossil assemblages from Upper Permian to lowermost Triassic in the western Dolomites (Italy). Memorie di Scienze Geologiche 34, 5–44.

Cirilli, S., Pirini Radrizzani, C., Ponton, M., Radrizzani, S., 1998. Stratigraphical and palaeoenvironmental analysis of the Permian-Triassic transition in the Badia Valley (Souther Alps, Italy). Palaeogeography, Palaeoclimatology, Palaeoecology 138, 85–113. https://doi.org/10.1016/S0031-0182(97)00123-5

Collin, P.Y., Kershaw, S., Tribovillard, N., Forel, M.B., Crasquin, S., 2015. Geochemistry of post-extinction microbialites as a powerful tool to assess the oxygenation of shallow marine water in the immediate aftermath of the end-Permian mass extinction. Int J Earth Sci (Geol Rundsch) 104, 1025–1037. https://doi.org/10.1007/s00531-014-1125-3

Crasquin, S., Perri, M.C., Nicora, A., Wever, P.D., 2008. Ostracods across the Permian-Triassic boundary in Western Tethys: The Bulla parastratotype (Southern Alps, Italy). Rivista italiana di Paleontologia e Stratigrafia Vol 114, No 2. https://doi.org/10.13130/2039-4942/5900

Dal Corso, J., Song, H., Callegaro, S., Chu, D., Sun, Y., Hilton, J., Grasby, S.E., Joachimski, M.M., Wignall, P.B., 2022. Environmental crises at the Permian–Triassic mass extinction. Nat Rev Earth Environ 3, 197–214. https://doi.org/10.1038/s43017-021-00259-4

Erwin, D.H., 1993. The Great Paleozoic Crisis: Life and Death in the Permian. Columbia University Press.

Farabegoli, E., Perri, M.C., Posenato, R., 2007. Environmental and biotic changes across the Permian–Triassic boundary in western Tethys: The Bulla parastratotype, Italy. Global and Planetary Change, Environmental and Biotic Changes during the Paleozoic-Mesozoic Transition 55, 109–135. https://doi.org/10.1016/j.gloplacha.2006.06.009

Foster, W.J., Danise, S., Price, G.D., Twitchett, R.J., 2017. Subsequent biotic crises delayed marine recovery following the late Permian mass extinction event in northern Italy. PLOS ONE 12, e0172321. https://doi.org/10.1371/journal.pone.0172321

Foster, W.J., Frank, A.B., Li, Q., Danise, S., Wang, X., Peckmann, J., 2024. Thermal and nutrient stress drove Permian-Triassic shallow marine extinctions. Cambridge Prisms: Extinction 1–25. https://doi.org/10.1017/ext.2024.9

Gliwa, J., Ghaderi, A., Leda, L., Schobben, M., Tomás, S., Foster, W.J., Forel, M.-B., Ghanizadeh Tabrizi, N., Grasby, S.E., Struck, U., Ashouri, A.R., Korn, D., 2020. Aras Valley (northwest Iran): high-resolution stratigraphy of a continuous central Tethyan Permian–Triassic boundary section. Fossil Record 23, 33–69. https://doi.org/10.5194/fr-23-33-2020

Grasby, S.E., Bond, D.P.G., 2023. How Large Igneous Provinces Have Killed Most Life on Earth—Numerous Times. Elements 19, 276–281. https://doi.org/10.2138/gselements.19.5.276

Grice, K., Cao, C., Love, G.D., Böttcher, M.E., Twitchett, R.J., Grosjean, E., Summons, R.E., Turgeon, S.C., Dunning, W., Jin, Y., 2005. Photic Zone Euxinia During the Permian-Triassic Superanoxic Event. Science. https://doi.org/10.1126/science.1104323

Groves, J.R., Rettori, R., Payne, J.L., Boyce, M.D., Altiner, D., 2007. End-Permian Mass Extinction of Lagenide Foraminifers in the Southern Alps (Northern Italy). Journal of Paleontology 81, 415–434.

Hays, L.E., Beatty, T., Henderson, C.M., Love, G.D., Summons, R.E., 2007. Evidence for photic zone euxinia through the end-Permian mass extinction in the Panthalassic Ocean (Peace River Basin, Western Canada). Palaeoworld, Contributions to Permian and Carboniferous Stratigraphy, Brachiopod Palaeontology and End-Permian Mass Extinctions, In Memory of Professor Yu-Gan Jin 16, 39–50. https://doi.org/10.1016/j.palwor.2007.05.008

Knies, J., Grasby, S.E., Beauchamp, B., Schubert, C.J., 2013. Water mass denitrification during the latest Permian extinction in the Sverdrup Basin, Arctic Canada. Geology 41, 167–170. https://doi.org/10.1130/G33816.1

Krewer, C., Poulton, S.W., Newton, R.J., März, C., Mills, B.J.W., Wagner, T., 2024. Controls on the Termination of Cretaceous Oceanic Anoxic Event 2 in the Tarfaya Basin, Morocco. American Journal of Science 324. https://doi.org/10.2475/001c.118797

Li, S., Wignall, P.B., Poulton, S.W., 2025. Co-application of rhenium, vanadium, uranium and molybdenum as paleo-redox proxies: Insight from modern and ancient environments. Chemical Geology 674, 122565. https://doi.org/10.1016/j.chemgeo.2024.122565

Loope, G.R., Kump, L.R., Arthur, M.A., 2013. Shallow water redox conditions from the Permian–Triassic boundary microbialite: The rare earth element and iodine geochemistry of carbonates from Turkey and South China. Chemical Geology 351, 195–208. https://doi.org/10.1016/j.chemgeo.2013.05.014

Mette, W., Roozbahani, P., 2012. Late Permian (Changsingian) ostracods of the Bellerophon Formation at Seis (Siusi) (Dolomites, Italy). Journal of Micropalaeontology 31, 73–87. https://doi.org/10.1144/0262-821X11-010

Posenato, R., 2019. The end-Permian mass extinction (EPME) and the Early Triassic biotic recovery in the western Dolomites (Italy): state of the art. Bollettino della Società Paleontologica Italiana 11–34. https://doi.org/10.4435/BSPI.2019.05

Poulton, S.W., Canfield, D.E., 2011. Ferruginous Conditions: A Dominant Feature of the Ocean through Earth's History. Elements 7, 107–112. https://doi.org/10.2113/gselements.7.2.107

Prinoth, H., Posenato, R., 2023. Bivalves from the Changhsingian (upper Permian) Bellerophon Formation of the Dolomites (Italy): ancestors of Lower Triassic post-extinction benthic communities. Papers in Palaeontology 9, e1486. https://doi.org/10.1002/spp2.1486

Proemse, B.C., Grasby, S.E., Wieser, M.E., Mayer, B., Beauchamp, B., 2013. Molybdenum isotopic evidence for oxic marine conditions during the latest Permian extinction. Geology 41, 967–970. https://doi.org/10.1130/G34466.1

Siegert, S., Kraus, S.H., Mette, W., Struck, U., Korte, C., 2011. Organic carbon isotope values from the Late Permian Seis/Siusi succession (Dolomites, Italy): Implications for palaeoenvironmental changes. Fossil Record 14, 207–217. https://doi.org/10.1002/mmng.201100008

Svensen, H.H., Jones, M.T., Mather, T.A., 2023. Large Igneous Provinces and the Release of Thermogenic Volatiles from Sedimentary Basins. Elements 19, 282–288. https://doi.org/10.2138/gselements.19.5.282

Tribovillard, N., Algeo, T.J., Baudin, F., Riboulleau, A., 2012. Analysis of marine environmental conditions based onmolybdenum–uranium covariation—Applications to Mesozoic paleoceanography. Chemical Geology, Special Issue Recent Advances in Trace Metal Applications to Paleoceanographic Studies 324–325, 46–58. https://doi.org/10.1016/j.chemgeo.2011.09.009

Twitchett, R.J., Wignall, P.B., 1996. Trace fossils and the aftermath of the Permo-Triassic mass extinction: evidence from northern Italy. Palaeogeography, Palaeoclimatology, Palaeoecology 124, 137–151. https://doi.org/10.1016/0031-0182(96)00008-9

Wignall, P.B., Twitchett, R.J., 1996. Oceanic Anoxia and the End Permian Mass Extinction. Science 272, 1155–1158. https://doi.org/10.1126/science.272.5265.1155

Xiang, L., Zhang, H., Schoepfer, S.D., Cao, C., Zheng, Q., Yuan, D., Cai, Y., Shen, S., 2020. Oceanic redox evolution around the end-Permian mass extinction at Meishan, South China. Palaeogeography, Palaeoclimatology, Palaeoecology 544, 109626. https://doi.org/10.1016/j.palaeo.2020.109626

Yang, F., Li, S., An, K.Y., Bond, D.P.G., Ao, R., Wu, X.B., Ma, L.L., Sun, Y.D., 2024. Re-Evaluating Water Column Reoxygenation During the End Permian Mass Extinction. Geochemistry, Geophysics, Geosystems 25, e2024GC011779. https://doi.org/10.1029/2024GC011779

Zhang, F., Shen, S., Cui, Y., Lenton, T.M., Dahl, T.W., Zhang, H., Zheng, Q., Wang, W., Krainer, K., Anbar, A.D., 2020. Two distinct episodes of marine anoxia during the Permian-Triassic crisis evidenced by uranium isotopes in marine dolostones. Geochimica et Cosmochimica Acta, New developments in geochemical proxies for paleoceanographic research 287, 165–179. https://doi.org/10.1016/j.gca.2020.01.032

FIGURE CAPTIONS

Fig. 1 (A) Paleogeographic map (WGS84) of the study area showing the location of Seis outlining the emerged land (yellow), marine environment (blue) and Periadriatic lineament (red line) (modified from Posenato, 2019). **(B)** Photograph of Seis, with the formation boundary marked in red. People for scale.

Fig. 2 Log of the Seis section, including paleontological observations made in the field. The colors reflect the rock color and the red band marks the PTME (following Farabegoli et al., 2007). The abbreviations m, w, p and g stand for mud-, wack-, pack- and grainstone, respectively, and OU, B and T for Ostracod Unit, Bulla Member and Tesero Member, respectively.

Fig. 3 Trends in $\delta^{13}C_{Carb}$ (Siegert et al., 2011), RSM EF*, Fe speciation (black arrows marking samples with iron <0.5wt%) and Th/U (Wignall and Twitchett, 1996 & this study) plotted next to the log of Seis. Gray circles mark published data, the vertical gray dashed lines represent no enrichment compared to PAAS, and the red dashed box marks the PTME.

Fig. 4 Comparison of EF_U* to EF_{Mo}*. The red arrows indicate different Mo accumulation pathways, with the redox variation trajectory illustrating benthic deoxygenation from oxic, throgh dysoxic and anoxic, to euxinic conditions and the particle shuttle (PS) the uptake of Mo

through redox cycling of oxyhydroxides (Tribovillard et al., 2012). The diagonal dotted lines represent proportions of the seawater (SW) Mo/U molar ratio.

[1]Supplemental Material. *Detailed methods description (S1.docx) and complete geochemical data set (S2.xlsx).* Please visit https://doi.org/10.1130/XXXX to access the supplemental material, and contact editing@geosociety.org with any questions.

FIGURES

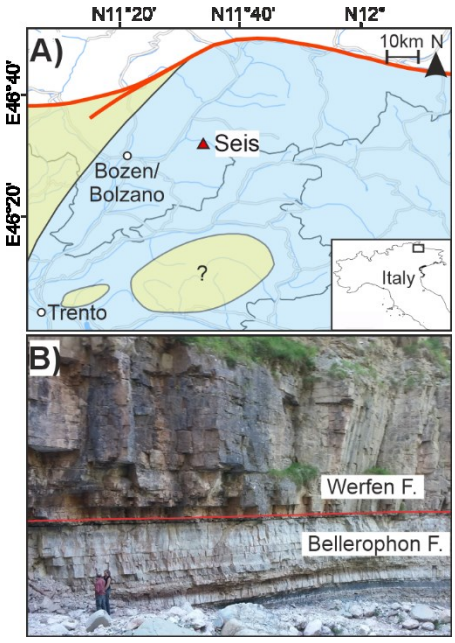

Fig. 2

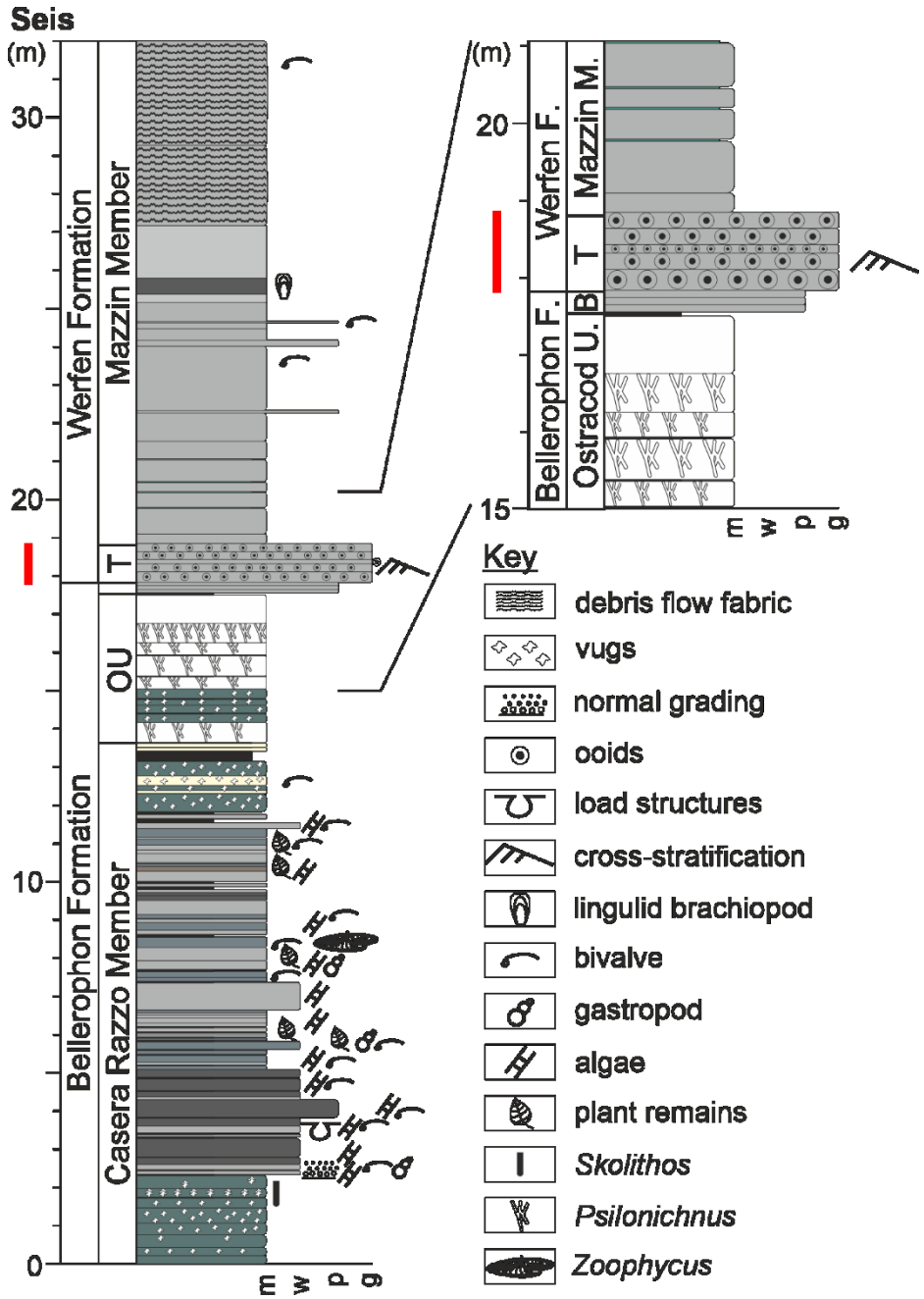
Seis
(m)
30
20
10
0
Werfen Formation
Mazzin Member
T
OU
Bellerophon Formation
Casera Razzo Member
E W P G
(m)
20
15
Werfen F.
Mazzin M.
T
B
Bellerophon F.
Ostracod U.
E W P G
Key
debris flow fabric
vugs
normal grading
ooids
load structures
cross-stratification
lingulid brachiopod
bivalve
gastropod
algae
plant remains
Skolithos
Psilonichnus
Zoophycus

Fig. 2

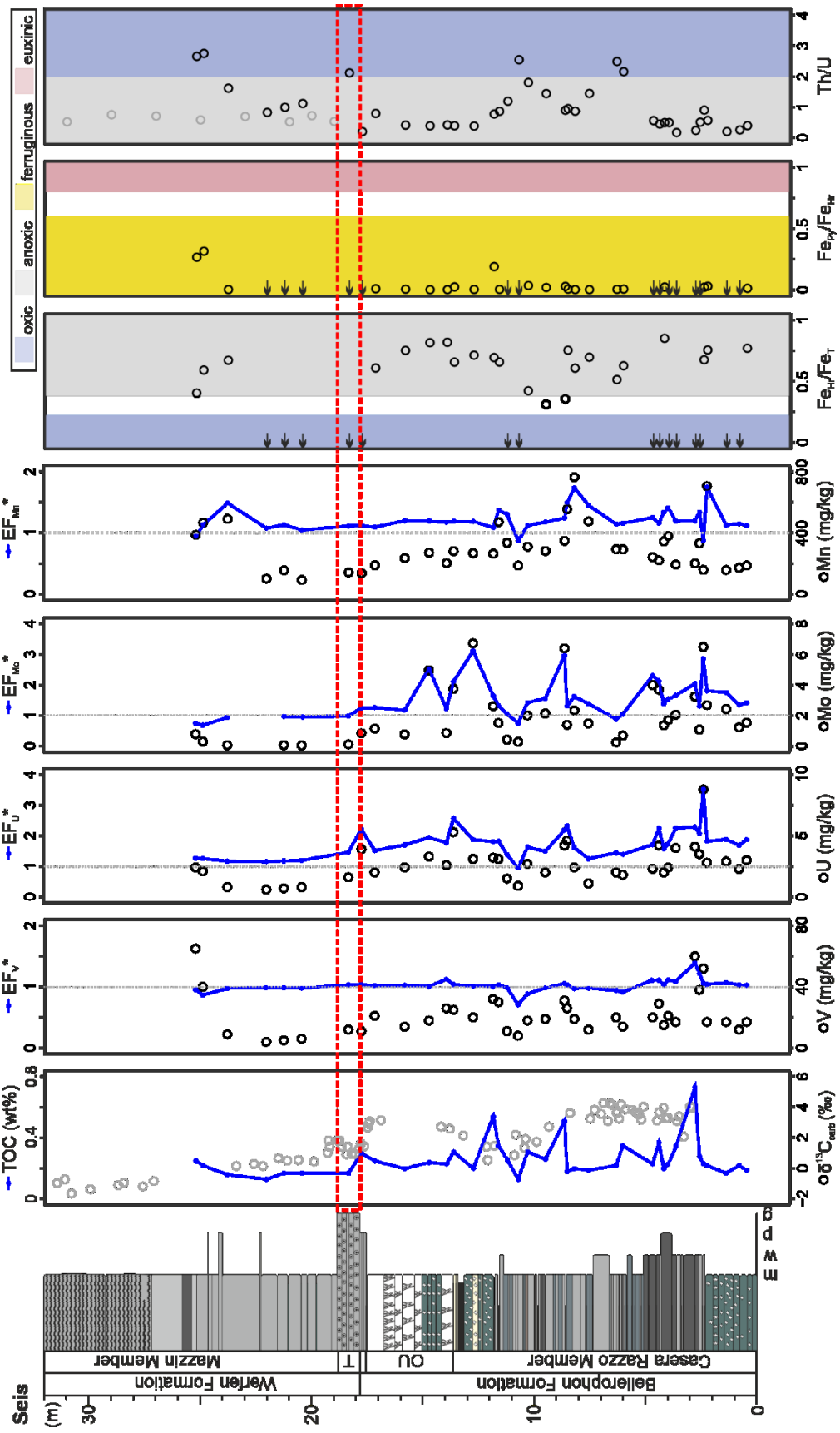
Seis
(m)
30
20
10
0
Wolfen Formation
Mazzin Member
T
OU
Bellerophon Formation
Casera Razzo Member
TOC (wt%)
δ13Ccarb (‰)
EFV*
oV (mg/kg)
EFU*
oU (mg/kg)
EFMo*
oMo (mg/kg)
EFMn*
oMn (mg/kg)
FeH/FeT
FePy/FeHR
Th/U
oxic
anoxic
ferruginous
euxinic

359

360 **Fig. 3**

361

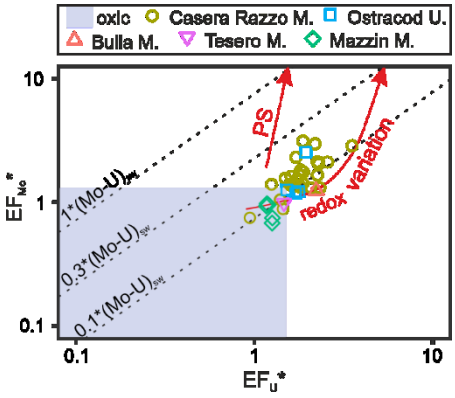

362

363 **Fig. 4**

364